Sulfidation Processes of PVP-Coated Silver Nanoparticles in Aqueous Solution: Impact on Dissolution Rate

Clément Levard,[†,‡,*] Brian C. Reinsch,[‡,§] F. Marc Michel,[†,∥] Camella Oumahi,[⊥] Gregory V. Lowry,[‡,§] and Gordon E. Brown, Jr.[†,‡,∥]

[†]Surface and Aqueous Geochemistry Group, Department of Geological & Environmental Sciences, Stanford University, Stanford, California 94305-2115, United States

[‡]Center for Environmental Implications of NanoTechnology (CEINT), P.O. Box 90287, Duke University, Durham, North Carolina 27708-0287, United States

[§]Department of Civil and Environmental Engineering, Carnegie Mellon University, Pittsburgh, Pennsylvania 15213, United States

[∥]Stanford Synchrotron Radiation Lightsource, SLAC National Accelerator Laboratory, 2575 Sand Hill Road, Menlo Park, California 94025, United States

[⊥]Department of Chemistry, Université Pierre et Marie Curie (Paris 6), Paris, France

S *Supporting Information*

ABSTRACT: Despite the increasing use of silver nanoparticles (Ag-NPs) in nanotechnology and their toxicity to invertebrates, the transformations and fate of Ag-NPs in the environment are poorly understood. This work focuses on the sulfidation processes of PVP-coated Ag-NPs, one of the most likely corrosion phenomena that may happen in the environment. The sulfur to Ag-NPs ratio was varied in order to control the extent of Ag-NPs transformation to silver sulfide (Ag_2S). A combination of synchrotron-based X-ray Diffraction (XRD) and Extended X-ray Absorption Fine Structure spectroscopy shows the increasing formation of Ag_2S with an increasing sulfur to Ag-NPs ratio. TEM observations show that Ag_2S forms nanobridges between the Ag-NPs leading to chain-like struc-

tures. In addition, sulfidation strongly affects surface properties of the Ag-NPs in terms of surface charge and dissolution rate. Both may affect the reactivity, transport, and toxicity of Ag-NPs in soils. In particular, the decrease of dissolution rate as a function of sulfide exposure may strongly limit Ag-NPs toxicity since released Ag^+ ions are known to be a major factor in the toxicity of Ag-NPs.
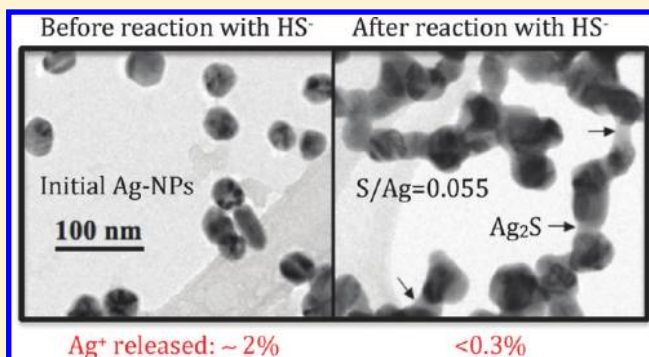
INTRODUCTION

Among the major types of manufactured nanoparticles (including C nanotubes, Au, TiO_2, and ZnO), silver nanoparticles (Ag-NPs) are currently the most widely used in the nanotechnology industry[1] in a variety of applications mainly for their unique antibacterial, antiviral, and antifungal properties.[2] As a result, there is a growing concern about the environmental impact of released Ag nanoparticles, particularly their unintended impact on organisms and ecosystems.[3]

Numerous studies have demonstrated the toxicity of Ag-NPs. For example, a study by Choi and Hu[4] showed that Ag-NPs in the 5 nm size range are toxic to nitrifying bacteria and conclude that they may interfere with wastewater treatment methods. However, it is not clear whether Ag-NPs or Ag^+ ions released from them, in addition to other factors, are responsible for the toxicity.[5−8] Recently, Sotiriou et al.[9] proposed that the antibacterial activity of Ag-NPs depends on their size. When Ag-NPs are small (<10 nm), the release of Ag^+ dominates the antibacterial activity of nanosilver. However,

when the particle size is >10 nm, released Ag^+ ions alone cannot completely explain the observed antimicrobial properties, and there is evidence for a Ag-NP-specific effect for the antibacterial activity of nanosilver.[10] Although these studies appear to be contradictory,[5−10] they all suggest that dissolved Ag species control part of the toxicity. Capping agents may also be an important factor, in addition to nanoparticle size, in controlling toxicity. For example, El Badawy et al.[11] recently suggested that the surface charge of 10−18 nm Ag-NPs, which was controlled by different capping agents (PVP, citrate, and polyethyleneimine), is responsible for their difference in toxicity to PolySeed (a Gram-positive bacillus species), with a more positive surface charge resulting in greater toxicity.

Most of these toxicity studies have not accurately represented environmental conditions because they have not considered transformations of Ag-NPs expected in different environments (e.g., oxidizing vs reducing) and therefore have not evaluated the environmentally relevant form of Ag-NPs. Environmental transformations of Ag-NPs need to be investigated to determine the change in their surface properties and reactivity (e.g., dissolution), which will, in turn, affect their transport, reactivity, and toxicity in soils and natural waters. Strangely, very few studies have focused on the environmental transformations of Ag-NPs.[12] The most common Ag corrosion product occurs when silver strongly reacts with reduced sulfur ligands to form a silver sulfide (Ag_2S) corrosion layer. Kim et al. recently discovered the presence of Ag_2S nanoparticles in sewage sludge products.[13] Although the source of Ag is uncertain, authors hypothesize that because naturally occurring crystals of Ag_2S are rare, Ag_2S nanoparticles are formed during wastewater treatment by the reaction of either Ag-NPs or soluble Ag ions with reduced sulfur species. The sulfidation processes for Ag-NPs have not been investigated as extensively as for their bulk counterpart.[14,15] Crucial differences between Ag-NPs and bulk silver are that Ag-NPs have a much higher surface to volume ratio and may have enhanced surface reactivity. Furthermore, Ag-NPs also have a polymer coating, which may also affect their behavior toward sulfide. Sulfidation of Ag-NPs in contact with laboratory air has been investigated which showed that a Ag_2S-Ag core—shell structure formed on the nanoparticles after a few weeks of exposure.[16] To the best of our knowledge, there have been no studies of the aqueous sulfidation of Ag-NPs.

The present work focuses on characterization of synthetic Ag-NPs that have been reacted with Na_2S, which resulted in significant changes in surface properties, aggregation state, surface charge, and dissolution rates. The Na_2S to Ag-NPs ratio was varied in order to control the depth of Ag-NPs transformation to Ag_2S. Analysis of reaction products was done using synchrotron-based X-ray Diffraction (XRD) and Extended X-ray Absorption Fine Structure spectroscopy (EXAFS), coupled with laboratory-based Transmission Electronic Microscopy (TEM), Scanning Electron Microscopy (SEM), and X-ray Photoelectron Spectroscopy (XPS). The results of this work allow us to hypothesize on the transport and toxicity behavior of Ag-NPs in natural systems.

■ MATERIALS AND METHODS

PVP-Coated Ag-NPs Synthesis. Ag-NPs were synthesized following a protocol adapted from Kim et al.[17] First, 13.5 g of polyvinylpyrrolidone (PVP, M_w = 10 000) was dissolved in 50 mL of ethylene glycol. After heating the solution to 140 °C, 3.15 g of $AgNO_3$ in deionized (DI) water (3 mL) was added to the ethylene glycol and reacted for 2 h. The solution was then cooled to 25 °C and the Ag-NPs were separated from the ethylene glycol using 100% acetone followed by centrifugation at a relative centrifugal force maximum value (RCF_{max}) of 26 040 g for 1 h. A final washing procedure was carried out twice in which the solution was washed with DI water and centrifuged again for 1 h.

Sulfidation of Ag-NPs. The Ag-NPs were sulfidized using a 10^{-3} M sodium sulfide (Na_2S) solution in a 0.01 M $NaNO_3$ electrolyte. To adjust the S/Ag ratio for the experiment, a fixed concentration of Na_2S was added to varying concentrations of pH 7 ± 0.2 Ag-NPs solutions (Table 1). After 24 h, the final solutions were centrifuged and washed with DI water. Finally, the

Table 1. Initial Concentrations of Ag-NPs and Corresponding S/Ag Ratio

conc. Ag-NPs (mol·L^{-1})	S/Ag (C_S = 0.001 mol·L^{-1})
0.0527	0.019
0.0267	0.037
0.0181	0.055
0.0137	0.073
0.0093	0.108
0.0046	0.216
0.0032	0.308
0.0023	0.432
0.0019	0.540
0.0014	0.719
0.0009	1.079

Ag-NPs were resuspended in DI water or dried depending on the type of analysis that followed.

Structural Characterization. Synchrotron radiation-based XRD data were collected for the Ag-NPs used in the present work at beamline 11-ID-B (λ = 0.2128 Å) at the Advanced Photon Source (APS), Argonne National Laboratory, using a Perkin-Elmer amorphous silicon detector. Samples were mounted in 1 mm Kapton capillaries. Images were integrated into intensity vs 2θ plots using the program Fit2D.[18] Rietveld refinement was carried out for phase quantification using the General Structure Analysis System (GSAS)[19] and EXPGUI.[20] Silver K-edge EXAFS spectra were collected at the Stanford Synchrotron Radiation Lightsource (SSRL) on wiggler beamline 11—2 at room temperature in transmission mode. An N_2-cooled Si(220) double crystal monochromator was detuned by 30% for harmonic rejection, and energy calibration was performed with a Ag metal foil placed after the I1 transmitted beam detector. Samples were diluted with glucose powder to achieve an optimized absorption jump of 1. EXAFS spectra of the following reference compounds were also collected: AgCl, $AgNO_3$, Ag_2S, AgO, Ag_2O, and Ag_2CO_3. Linear combination fitting (LCF) of the EXAFS data was performed using the SIXPack interface[21] to the IFEFFIT XAFS analysis package.[22] TEM images were acquired using a FEI Tecnai G2 F20 X-TWIN (accelerating voltage of 200 kV) equipped with a CCD camera. A dilute suspension of Ag-NPs in DI water was deposited on a copper TEM grid covered by an ultrathin carbon support film. The TEM grid was dried under ambient air before TEM observations. SEM images of the initial Ag-NPs before sulfidation were collected with a FEI-XL30 Sirion SEM (accelerating voltage of 5 kV). For XPS analysis, samples in aqueous solution were deposited on a silicon wafer and dried in air; a PHI VersaProbe Scanning XPS Microprobe was used for these measurements. In addition, total carbon in the samples was measured using an Elemental Analyzer (Carlo-Erba NA 1500 analyzer).

ζ Potential and Solubility Measurements. Aqueous solutions containing 0.1 g·L^{-1} Ag-NPs in 0.01 M $NaNO_3$ were prepared at different pH values ranging from 2 to 12 for ζ potential measurements. NaOH and HNO_3 were used to adjust the pH to the desired value. The solutions were equilibrated for 72 h before analysis. The ζ potential was measured using a Malvern ZetaSizer NanoSeries. Aqueous solutions containing 1 g·L^{-1} of Ag-NPs at pH 7 ± 0.2 were prepared in a 0.01 M $NaNO_3$ electrolyte for dissolution rate measurements. The amount of released Ag^+ was measured using an Inductively
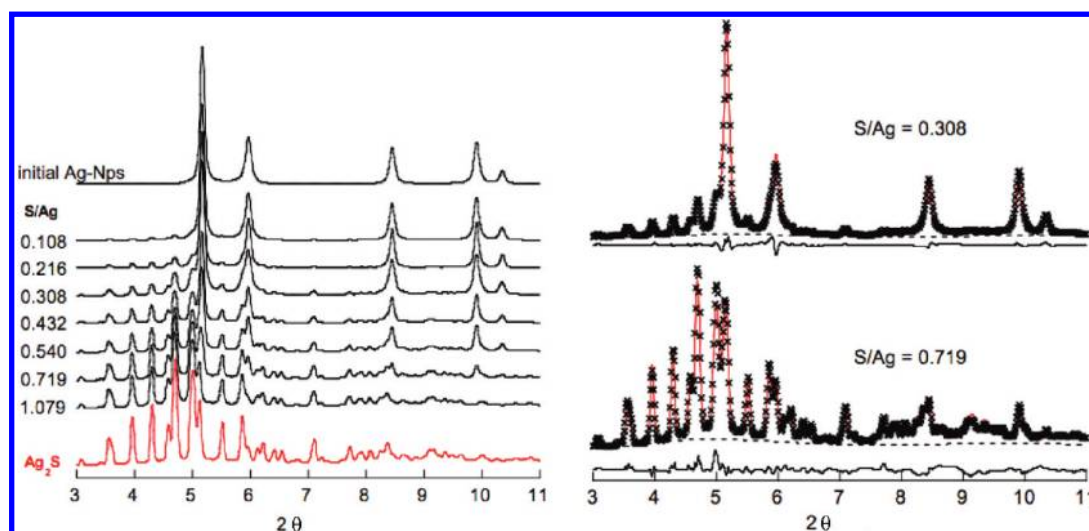
Figure 1. (Left) XRD patterns of the synthetic Ag-NPs before and after reaction with aqueous Na_2S for S/Ag ratio ranging from 0.108 to 1.079; (Right) Two examples of Rietveld fitting (other XRD patterns and fits are presented in Figure S4 of the SI).

Coupled Plasma Spectrometer (ICP)(TJA IRIS Advantage/1000 Radial ICAP Spectrometer) at different times (from $t = 0$ to $t = 30$ days) in the supernatant after centrifugation of the solution at an RCF_{max} value of 208 429 $\times g$ for 45 min. Three replicates of each sample were run for statistical purposes.

RESULTS AND DISCUSSION

Structural Characterization of the Initially Synthesized Ag-NPs. The synthesized Ag-NPs are quasi-spherical in shape, with an average size obtained from SEM image analysis of 39 ± 9 nm (Figure S1 of the Supporting Information, SI). XRD data show (Figure 1) that Ag-NPs crystallize with a fcc structure matching that of metallic bulk silver (ICSD-64706). No other crystalline phases were detected. Surface charges of the nanoparticles were measured and are uniformly negative between pH 2 and 12 (Figure S2 of the SI). The PVP capping agent was characterized by C_{1s} XPS. The C_{1s} peak was deconvoluted into three peaks with binding energies of 284.7, 285.8, and 287.6 eV (Figure S1 of the SI). These contributions were attributed to the three configurations of C in the PVP molecule.[16] The total amount of carbon adsorbed on the Ag-NPs (part of the PVP) represents about 1.4% in mass of the total product (Figure S3 of the SI).

Sulfidation of Ag-NPs: Characterization of the Reaction Product. Two complementary synchrotron-based experiments were performed to quantify and identify the new phase(s) forming after reaction with aqueous Na_2S: (i) XRD, which is sensitive to the presence of crystalline phases, and (ii) EXAFS spectroscopic data collected at the Ag−K edge, which is sensitive to the local structural environment of Ag in all Ag-bearing phases (crystalline or otherwise).

XRD analysis showed the presence of an additional phase after reaction with aqueous Na_2S, and the peak intensities of this new phase gradually increased as the S/Ag ratio increased (Figure 1, left). This new phase was identified as silver sulfide (Ag_2S), which is known as acanthite. The PVP capping agent does not protect the Ag-NPs from corrosion, as was also found in a previous study of the corrosion of Ag-NPs in air.[16] This finding is consistent with expectations for an adsorbed polymer coating as this adsorption

technique provides incomplete surface coverage of the nanoparticles.[23] Furthermore, sulfidation of the Ag-NPs resulted in a decrease of carbon on the NP surfaces (Figure S3), presumably due to loss of coating as discussed later. Rietveld analysis was performed in order to quantify the amount of Ag_2S formed as a function of S/Ag ratio. Two examples of the fitting are shown in Figure 1 (right). Significant amounts of Ag_2S (more than 1%) were observed for Ag-NPs with S/Ag ratio ≥ 0.055 (Figure 1 and Figure S4 of the SI). Also, metallic silver was absent for Ag-NPs with S/Ag = 1.079. The sensitivity of XRD to minor amounts of Ag_2S formed at the lower S/Ag ratios is limited to ~ 1 wt %. The sensitivity is less in the case of a minor fraction of Ag_2S forming exclusively with short-range structural order since these do not manifest well-defined diffraction maxima. In this context, EXAFS spectroscopy collected at the Ag K-edge is a good complementary technique because it is sensitive to all Ag-bearing phases and is independent of their degree of crystallinity.

Linear combination fitting of the EXAFS spectra of Ag-NPs after reaction with Na_2S-containing aqueous solutions was performed using EXAFS spectra of the two phases identified by XRD (Ag^0 and Ag_2S). These two components were sufficient to obtain good linear combination fits up to $k = 15$ Å^{-1} (Figure 2 (left) and Figure S5 of the SI). The quality of the fits, illustrated by the small residuals (Figure S5 and Table S2 of the SI), strongly suggests that no other significant Ag-bearing phases are present on this set of samples. Adding other components such as Ag_2O did not improve the fits significantly. The percentage of Ag_2S obtained from the linear combination fitting is plotted in Figure 2 (right) and compared with the percentages of the two crystalline phases (Ag^0 and Ag_2S) obtained from XRD Rietveld analysis (Figure 2 and Table S1 of the SI).

The amount of Ag_2S obtained from linear combination fitting of the Ag-NPs EXAFS spectra is greater than the amount obtained from Rietveld analysis of the XRD data at all the S/Ag ratios evaluated. This finding strongly suggests that part of the Ag_2S is amorphous (with a local structure around Ag similar to the local structure of Ag in acanthite) and this phase is detected by EXAFS spectroscopy but not by XRD analysis.

From the combination of XRD and EXAFS results it is possible to evaluate the fractions of crystalline and amorphous
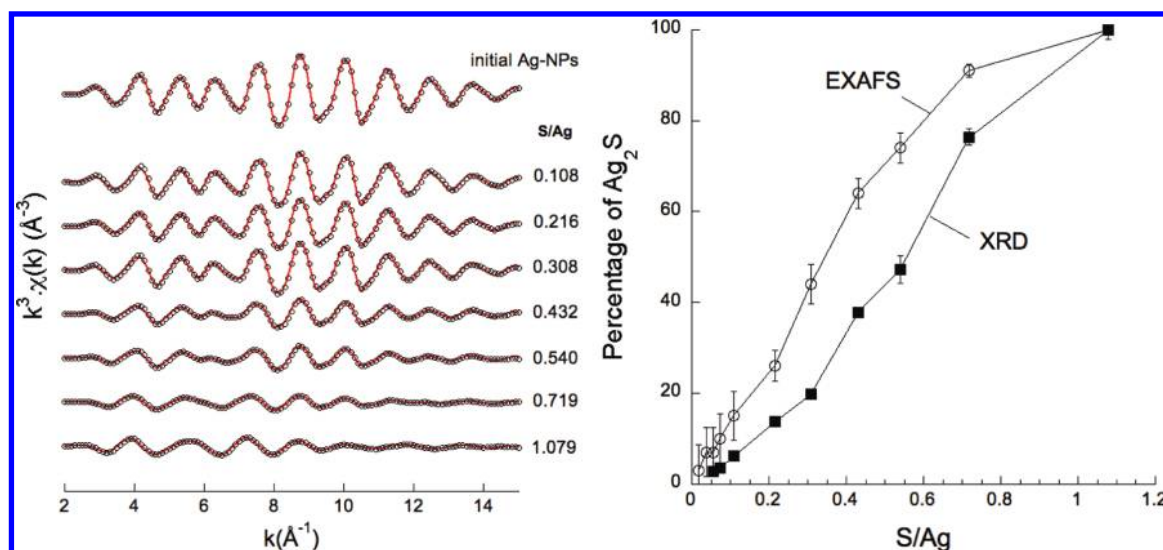
Figure 2. (Left) Experimental EXAFS spectra (dots) and linear combination fits (red lines) of Ag-NPs samples before and after reaction with aqueous Na$_2$S for S/Ag ratio ranging from 0.108 to 1.079. Other EXAFS spectra, fits and difference plots are presented in Figure S5 of the SI. (Right) Ag$_2$S percentages obtained from Rietveld analysis (squares) and from LCF of the EXAFS spectra (circles) as a function of S/Ag ratio.
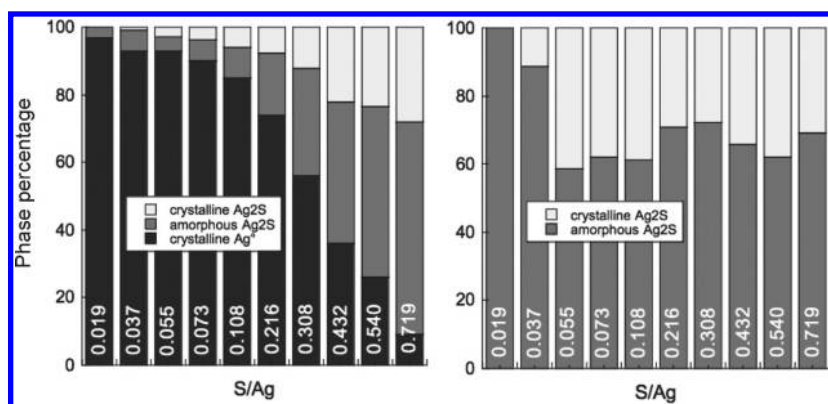

Figure 3. (Left) Percentages of Ag^0 and crystalline/amorphous Ag$_2$S as a function of S/Ag ratio. (Right) Proportions of crystalline and amorphous Ag$_2$S as a function of S/Ag ratio.

Ag$_2$S for each S/Ag ratio using the expression:

$$x_{Ag°}/x_{Ag2S} = a \qquad (1)$$

where $x_{Ag°}$ and x_{Ag2S} are the crystalline fractions of each species obtained from the Rietveld analysis of the XRD data. In addition:

$$x_{Ag°} + y_{Ag°} = b \qquad (2)$$

$$x_{Ag2S} + y_{Ag2S} = 1 - b \qquad (3)$$

where $y_{Ag°}$ and y_{Ag2S} are the fractions of silver with only short-range order for the two phases and b is obtained from the LCF of the EXAFS spectra. Assuming that $y_{Ag°} = 0$ (i.e., all of the metallic silver is crystalline), the three fractions $x_{Ag°}$, x_{Ag2S}, and y_{Ag2S} were calculated for each S/Ag ratio and are plotted in Figure 3 (left). Here the gradual transformation of Ag^0 to Ag$_2$S is apparent.

Interestingly, the ratio of amorphous to crystalline Ag$_2$S (Figure 3, right) remains approximately constant at about 2 to 1 for S/Ag ratios >0.055. A possible explanation for this constant ratio could be a poisoning effect on the Ag$_2$S crystal growth caused by desorbed PVP. The same experiments performed on

uncoated Ag-NPs would be necessary to confirm this hypothesis, and such experiments are underway. For Ag-NPs samples exposed to low S/Ag ratios ($\leq$0.037), Ag$_2$S is mostly or totally amorphous or so poorly crystalline that they do not produce diffraction features of sufficient intensity to detect.

TEM was performed on the initial and sulfidized Ag-NPs. Figure 4a−f shows TEM images of Ag-NPs in order of increasing sulfide exposure. Initially, the Ag-NPs are fairly dispersed even if small aggregates of very few particles were observed probably due to the drying process during the grid preparation (Figure 4a). As soon as a small amount of sulfur is added to the system (S/Ag = 0.019), particles strongly aggregate forming chain-like structures (Figure 4b). Similar structures were found to form when Ag-NPs reacts with Cl.[12] As the sulfidation rate increases, one can observe the formation of small bridges between Ag-NPs (indicated by arrows in Figure 4c,d). These bridges, not visible for the lower S/Ag ratio, appear to be longer and more and more present in the system as the S/Ag ratio increases. For high sulfidation ratio, S/Ag = 0.540 and 1.079 (Figure 4e,f), the initial spheres are less and less apparent and finally lead to an amorphous, unshaped product.
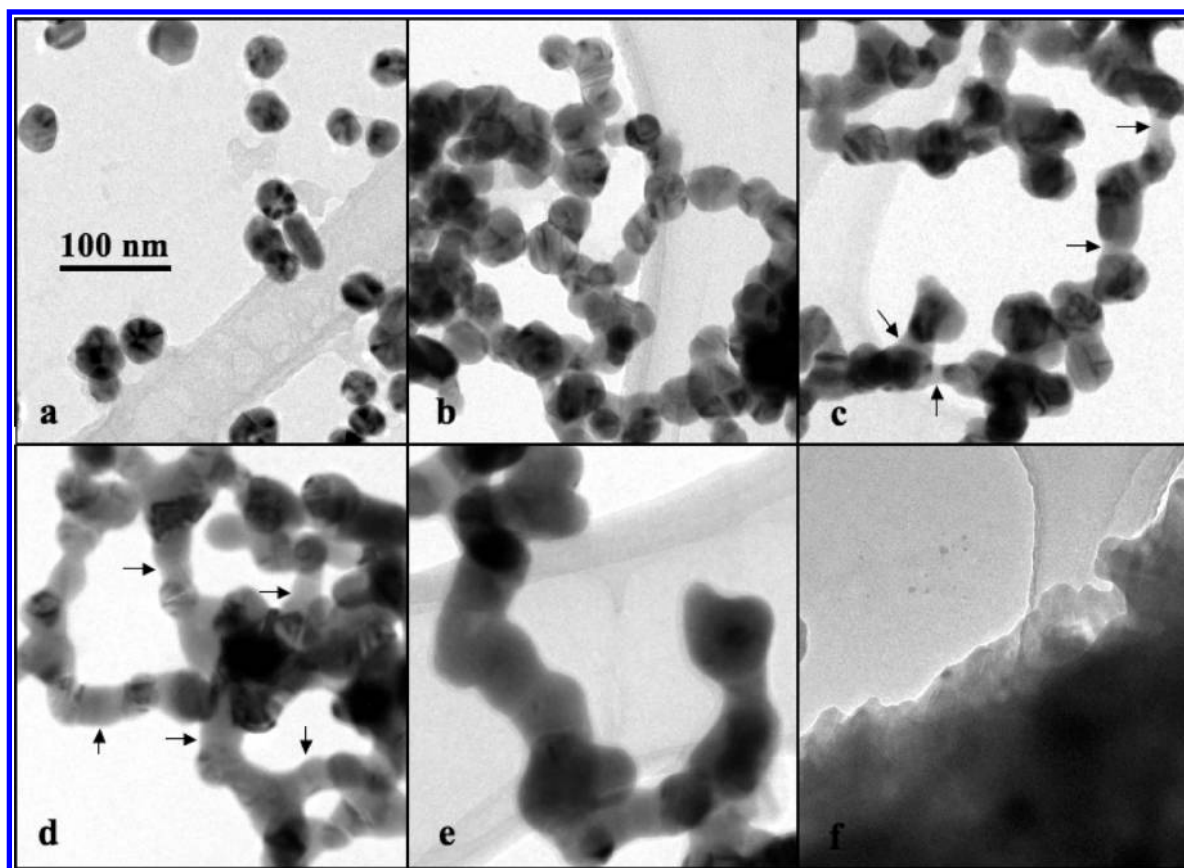
Figure 4. TEM images of the initial and sulfidized synthetic Ag-NPs: (a) initial; (b) S/Ag = 0.019; (c) S/Ag = 0.055; (d) S/Ag = 0.308; (e) S/Ag = 0.540; and (f) S/Ag = 1.079. Magnification is identical for all six images.
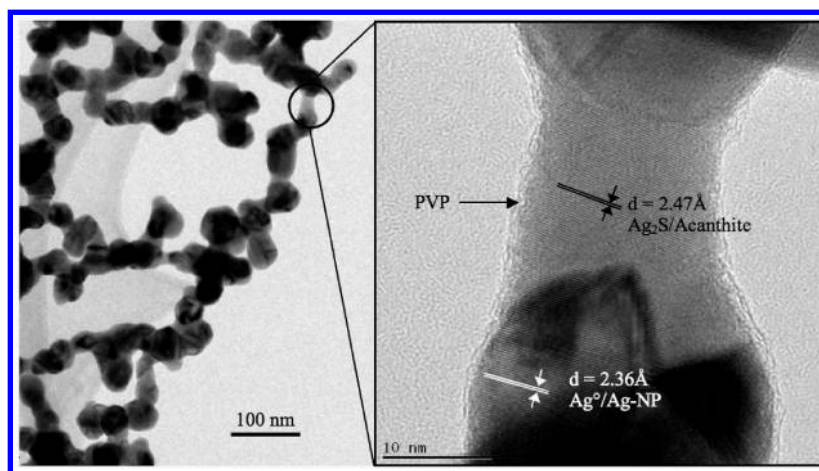

Figure 5. TEM images for S/Ag = 0.055. The right image is at higher magnification and is centered on one of the nanobridges observed at low magnification (left image).

Higher resolution TEM images were necessary to identify the phase forming the bridges between the quasi-spherical particles. We were able to distinguish lattice fringe spacings characteristic of the two crystalline phases identified by XRD (Figure 5). One phase consists of Ag° NPs, which are easily distinguishable in the TEM images because of their quasi-spherical shapes, twinned aspect, and high contrast. The lattice fringe spacing of these nanoparticles is consistent with the (111) lattice planes of the fcc structure of metallic silver identified by XRD (2.4 Å). The second phase has lower contrast and forms nanobridges between the quasi-spherical Ag-NPs. The lattice fringe spacing associated with this second phase is 2.6 Å, which matches with the (−121) planes of the Ag_2S structure identified by XRD (relative intensity of 100%).

Analysis of the TEM images suggests that metallic silver is oxidized through the reaction with sulfur, dissolves in part, and
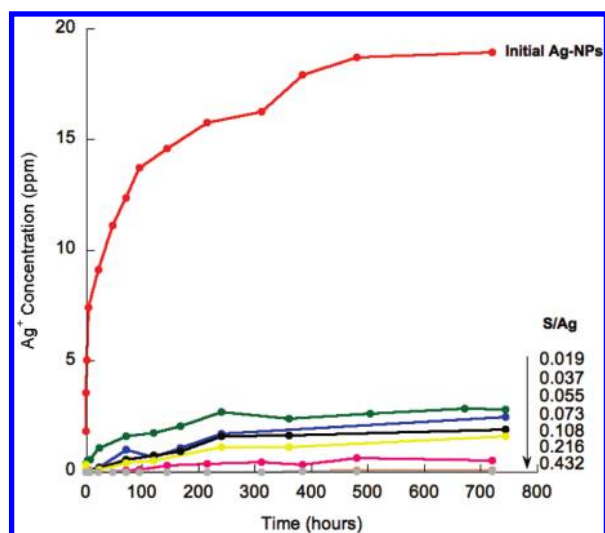
Figure 6. Dissolution rate measurements of Ag-NPs before and after reaction with increasing concentrations of aqueous Na$_2$S. (Initial Ag-NPs concentration for dissolution rate measurements was 1000 ppm in 0.01 M NaNO$_3$, pH = 7).

reprecipitates as Ag$_2$S nanobridges between nanoparticles. This morphology is different from that observed previously for silver nanoparticles and nanowires exposed to air in the laboratory and to H$_2$S, which produced a Ag—Ag$_2$S core—shell nanostructure.[16] In our case, water seems to play a significant role in determining the final morphology of the sulfidized Ag-NPs, perhaps acting as a transport medium for dissolved species. In the case of air corrosion, with more limited transport of oxidized/dissolved Ag species, Ag$_2$S precipitation occurs at the surface of the Ag-NPs, forming a Ag—Ag$_2$S core—shell structure. In addition to the Ag$_2$S nanobridges, Ag—Ag$_2$S core—shell structures are also observed by TEM for some of the nanoparticles based on contrast differences between Ag^0 and Ag$_2$S, especially in systems with higher S/Ag (cf., e.g., Figure 4e).

Loss of the Organic Capping Agent (PVP) during Sulfidation. Formation of Ag$_2$S nanobridges between Ag-NPs accompanying their sulfidation demonstrates that the PVP coating, which usually serves to prevent aggregation, does not inhibit sulfidation and does not prevent aggregation of the Ag-NPs following sulfidation. The total amount of carbon in the samples was measured with a CN elemental analyzer (Figure S3 of the SI). Sulfidation of the Ag-NPs is accompanied by loss of part of the PVP capping agent. Indeed, the wt % of carbon decreases with increasing S/Ag ratio, which is consistent with an aggregation process and a decrease of the specific surface area. The amount of carbon plateaus at approximately 0.6 wt.% as the S/Ag ratio increases. TEM images (Figure 5) show evidence for an amorphous-like layer with lower contrast at the edges of the Ag$_2$S nanobridges, which we interpret as indicating that the PVP desorbs initially but resorbs on the freshly precipitated Ag$_2$S nanobridges. In addition, sulfidized Ag-NPs have been analyzed by XPS to confirm the presence of PVP. The spectra presented in Figure S3 of the SI are consistent with the structure of initial PVP and can be fit with the three contributions reported earlier as characteristic of the PVP structure. Peak intensity variations can be interpreted as small changes in the amounts of these three species caused by the sulfidation process.

Surface Charge and Dissolution Rates of the Ag-NPs before and after Sulfidation. An important question examined in this work concerns how sulfidation affects Ag-NPs surface properties and consequently their behavior in natural systems. The ζ potentials were measured for Ag-NPs exposed to different S/Ag ratios (Figure S2 of the SI). The surface charge of the initial Ag-NPs is uniformly negative over the pH range studied (2 to 12). However, after sulfidation, the pH$_{PZC}$ of the sulfidated Ag-NPs increases with increasing S/Ag ratio. The measured pH$_{PZC}$ is ~5 for Ag-NPs exposed to S/Ag ratios 0.108 and 0.216 and ~7 for those exposed to S/Ag = 0.432. Further interpretation of the observed surface charge evolution is difficult because information on the PVP structure and Ag surface composition before and after sulfidation is currently lacking (see SI for additional details).

Release of ionic silver species appears to be one of the most important parameters to consider in terms of risk assessment because it governs, in part, Ag-NPs toxicity. The dissolution rates of the Ag-NPs were measured for different S/Ag ratios (Figure 6). Equilibrium for the initial Ag-NPs was reached after a month, and the quantity of dissolved Ag$^+$ species represented about 20 ppm, or 2% of the silver present initially within the Ag-NPs (initial concentration of Ag-NPs was 1000 ppm). Dissolution rates showed a strong decrease following sulfidation of the Ag-NPs. Even a S/Ag ratio as low as 0.019 leads to a decrease of Ag$^+$ species in solution by a factor of about 7 (3 ppm). As the S/Ag ratio increases, the dissolution rate decreases until Ag$^+$ could not be detected at S/Ag > 0.432. This result is consistent with the low solubility constant for Ag$_2$S ($K_{sp} = 10^{-50}$).[24,25]

Implications of Sulfidation Processes for the Behavior of Ag-NPs in Reducing Environments. Sulfidation strongly affected the properties of the Ag-NPs in our study including aggregation state, surface charge, adsorbed mass of coating, and release of Ag$^+$ ion. Each of these properties will affect the fate, transport, and toxicity of Ag NPs in the environment. Strong aggregation of the particles following sulfidation was observed by TEM. A recent review paper highlighted the importance of aggregation effects on transport and reactivity of NPs in ground and surface water.[26] Deposition and sedimentation processes were found to considerably limit the mobility of the NPs in ground and surface water, respectively. Thus, the increased aggregation of sulfidized Ag-NPs suggests that sulfidation will decrease the mobility of Ag-NPs in reducing environments. Modification of the surface charge and loss of the PVP coating may also impact the aggregation and transport of Ag-NPs as well as their interactions with organisms in soils. An organic coating at the surface of nanoscale zerovalent iron was been shown to limit interactions of these NPs with *Escherichia coli* partly because of electrostatic repulsions between the negatively charges NPs and the negative charge of the outer membrane of the bacteria.[27] El Badawy et al. [11] suggest that surface charge is one of the most important factors governing the toxicity of Ag-NPs. Finally, the observed decrease of dissolution rate as a function of sulfide exposure may strongly limit Ag-NPs toxicity because released Ag$^+$ ions are known to be a major factor in the toxicity of Ag-NPs.[3,9] This hypothesis is currently being tested for *E. coli*. Our results show that sulfidation processes may reduce the potential risk of Ag-NPs in reducing environments. However, the stability of this newly formed product has to be investigated over time, in particular, because the stability of an amorphous Ag$_2$S phase under different pH and redox conditions is currently unknown.

5265

dx.doi.org/10.1021/es2007758 |*Environ. Sci. Technol.* 2011, 45, 5260–5266

■ ASSOCIATED CONTENT

⑤ Supporting Information. SEM of the initial product, C1s XPS spectra, total carbon and surface charge as a function of S/Ag, experimental XRD patterns and Rietveld fitting, experimental EXAFS spectra and LSF fitting. This material is available free of charge via the Internet at http://pubs.acs.org.

■ AUTHOR INFORMATION

Corresponding Author
*Phone: 650-723-7513; e-mail: clevard@stanford.edu.

■ ACKNOWLEDGMENT

■ REFERENCES

(1) Rejeski, D.; Kulken, T.; Pollschuk, P.; Pauwels, E., *The project on emerging nanotechnologies*. http://www.nanotechproject.org/inventories/consumer/analysis_draft/, 2010.

(2) Lok, C. N.; Ho, C. M.; Chen, R.; He, Q. Y.; Yu, W. Y.; Sun, H.; Tam, P. K. H.; Chiu, J. F.; Che, C. M. Silver nanoparticles: partial oxidation and antibacterial activities. *J. Biol. Inorg. Chem.* **2007**, *12* (4), 527–534.

(3) Luoma, S. N. *Silver Nanotechnologies and the Environment: Old Problems or New Challenges*; Woodrow Wilson International Center for Scholars: Washington, DC, 2008.

(4) Choi, O.; Hu, Z. Q. Size dependent and reactive oxygen species related nanosilver toxicity to nitrifying bacteria. *Environ. Sci. Technol.* **2008**, *42* (12), 4583–4588.

(5) Navarro, E.; Piccapietra, F.; Wagner, B.; Marconi, F.; Kaegi, R.; Odzak, N.; Sigg, L.; Behra, R. Toxicity of silver nanoparticles to *Chlamydomonas reinhardtii*. *Environ. Sci. Technol.* **2008**, *42* (23), 8959–8964.

(6) Asharani, P. V.; Wu, Y. L.; Gong, Z.; Valiyaveettil, S. Toxicity of silver nanoparticles in zebrafish models. *Nanotechnology* **2008**, *19* (25), 255102.

(7) Fabrega, J.; Fawcett, S. R.; Renshaw, J. C.; Lead, J. R. Silver nanoparticle impact on bacterial growth: effect of pH, concentration, and organic matter. *Environ. Sci. Technol.* **2009**, *43* (19), 7285–7290.

(8) Kawata, K.; Osawa, M.; Okabe, S. In vitro toxicity of silver nanoparticles at noncytotoxic doses to HepG2humanhepatoma cells. *Environ. Sci. Technol.* **2009**, *43* (15), 6046–6051.

(9) Sotiriou, G. A.; Pratsinis, S. E. Antibacterial activity of nanosilver ions and particles. *Environ. Sci. Technol.* **2010**, *44* (14), 5649–5654.

(10) Marambio-Jones, C.; Hoek, E. M. V. A review of the antibacterial effects of silver nanomaterials and potential implications for human health and the environment. *J. Nanopart. Res.* **2010**, *12* (5), 1531–1551.

(11) El Badawy, A. M.; Silva, R. G.; Morris, B.; Scheckel, K. G.; Suidan, M. T.; Tolaymat, T. M. Surface charge-dependent toxicity of silver nanoparticles. *Environ. Sci. Technol.* **2011**, *45* (1), 283–287.

(12) Li, X.; Lenhart, J. J.; Walker, H. W. Dissolution-accompanied aggregation kinetics of silver nanoparticles. *Langmuir* **2010**, *26* (22), 16690–16698.

(13) Kim, B.; Park, C. S.; Murayama, M.; Hochella, M. F., Jr. Discovery and characterization of silver sulfide nanoparticles in final sewage sludge products. *Environ. Sci. Technol.* **2010**, *44* (19), 7509–7514.

(14) Kleber, C.; Wiesinger, R.; Schnoller, J.; Hilfrich, U.; Hutter, H.; Schreiner, M. Initial oxidation of silver surfaces by S_2^- and S_4^+ species. *Corros. Sci.* **2008**, *50* (4), 1112–1121.

(15) Graedel, T. E.; Franey, J. P.; Gualtieri, G. J.; Kammlott, G. W.; Malm, D. L. On the Mechanism of Silver and Copper Sulfidation by Atmospheric H_2S and OCS. *Corros. Sci.* **1985**, *25* (12), 1163–1180.

(16) Elechiguerra, J. L.; Larios-Lopez, L.; Liu, C.; Garcia-Gutierrez, D.; Camacho-Bragado, A.; Yacaman, M. J. Corrosion at the nanoscale: The case of silver nanowires and nanoparticles. *Chem. Mater.* **2005**, *17* (24), 6042–6052.

(17) Kim, D.; Jeong, S.; Moon, J. Synthesis of silver nanoparticles using the polyol process and the influence of precursor injection. *Nanotechnology* **2006**, *17*, 4019–4024.

(18) Hammersley, A. P.; Svensson, S. O.; Hanfland, M.; Fitch, A. N.; Hausermann, D. Two-dimensional detector software: From real detector to idealised image or two-theta scan. *High Press. Res.* **1996**, *14* (4−6), 235–248.

(19) Larson, A. C.; Von Dreele, R. B., General Structure Analysis System (GSAS). In *Los Alamos National Laboratory Report LAUR* 2004; pp 86-748.

(20) Toby, B. H. EXPGUI, a graphical user interface for GSAS. *J. Appl. Crystallogr.* **2001**, *34*, 210–213.

(21) Webb, S. M. SIXpack: a graphical user interface for XAS analysis using IFEFFIT. *Phys. Scr.* **2005**, *T115*, 1011–1014.

(22) Newville, M. IFEFFIT: interactive XAFS analysis and FEFF fitting. *J. Synchrotron Rad.* **2001**, *8*, 322–324.

(23) Phenrat, T.; Liu, Y.; Tilton, R. D.; Lowry, G. V. Adsorbed polyelectrolyte coatings decrease Fe0 nanoparticle reactivity with TCE in water: Conceptual model and mechanisms. *Environ. Sci. Technol.* **2009**, *43* (5), 1507–1514.

(24) Ma, D. K.; Hu, X. K.; Zhou, H. Y.; Zhang, J. H.; Qian, Y. T. Shape-controlled synthesis and formation mechanism of nanoparticles-assembled Ag_2S nanorods and nanotubes. *J. Cryst. Growth* **2007**, *304* (1), 163–168.

(25) Graedel, T. E. Corrosion Mechanisms for Silver Exposed to the Atmosphere. *J. Electrochem. Soc.* **1992**, *139* (7), 1963–1970.

(26) Hotze, E. M.; Phenrat, T.; Lowry, G. V. Nanoparticle aggregation: Challenges to understanding transport and reactivity in the environment. *J. Environ. Qual.* **2010**, *39* (6), 1909–1924.

(27) Li, Z.; Greden, K.; Alvarez, P. J. J.; Gregory, K. B.; Lowry, G. V. Adsorbed polymer and NOM limits adhesion and toxicity of nano scale zerovalent iron to *E. coli*. *Environ. Sci. Technol.* **2010**, *44* (9), 3462–3467.